

Room-Temperature Ferromagnetism in Carbon-Doped ZnO

H. Pan,¹ J. B. Yi,^{2,*} L. Shen,¹ R. Q. Wu,¹ J. H. Yang,¹ J. Y. Lin,^{1,3} Y. P. Feng,^{1,†} J. Ding,^{2,‡} L. H. Van,² and J. H. Yin²

¹Department of Physics, National University of Singapore, 2 Science Drive 3, Singapore 117542

²Department of Materials Science and Engineering, National University of Singapore, 9 Engineering Drive 1, Singapore 117576

³Institute of Chemical and Engineering Sciences, 1 Pesek Road, Jurong Island, Singapore 627833

(Received 9 October 2006; revised manuscript received 19 January 2007; published 17 September 2007)

We report ferromagnetism in carbon-doped ZnO. Our first-principles calculations based on density functional theory predicted a magnetic moment of $2.02\mu_B$ per carbon when carbon substitutes oxygen in ZnO, and an ferromagnetic coupling among magnetic moments of the carbon dopants. The theoretical prediction was confirmed experimentally. C-doped ZnO films deposited by pulsed-laser deposition showed ferromagnetism with Curie temperatures higher than 400 K. The measured magnetic moment based on the content of carbide in the films [$(1.5\text{--}3.0)\mu_B$ per carbon] was in agreement with the theoretical prediction. The magnetism is due to the Zn-C system in the ZnO environment.

DOI: [10.1103/PhysRevLett.99.127201](https://doi.org/10.1103/PhysRevLett.99.127201)

PACS numbers: 75.50.Pp, 71.15.Mb, 75.47.-m

Dilute magnetic semiconductor (DMS) has attracted wide interest and there has been a major effort to produce DMSs with Curie temperatures (T_C) at or above room temperature. However, synthesis of such materials has been a challenge. DMS is usually produced by doping semiconductors with transition metals (TMs). ZnO and GaN were theoretically predicted to be ideal candidates for room-temperature DMS [1]. Even though ferromagnetism has been observed in a number of systems, experimental studies on TM-doped ZnO have produced inconsistent results and the mechanism of ferromagnetism in TM-doped ZnO remains unclear. It is speculated that TM dopants in ZnO form clusters or secondary phases, which are detrimental to applications of DMS. This promoted search for DMS based on alternative dopants. If non-TM dopants can be incorporated into ZnO and induce magnetism, DMS thus produced would not suffer from problems related to precipitates of dopants since they do not contribute to ferromagnetism. For example, copper doping in ZnO and GaN have been investigated and it has been confirmed experimentally that both Cu-doped ZnO and GaN are room-temperature DMSs [2–5].

Ferromagnetism was also reported in a number of carbon systems [6–10]. Some of these studies have speculated that intrinsic carbon defects could be responsible for the observed magnetic properties. Carbon adatoms on carbon nanotubes [11] and carbon substitutional doping in boron nitride nanotubes [12] were predicted to induce magnetism in the respective systems. It is therefore of interest to investigate the effect of carbon doping in ZnO and explore the possibility of using carbon as a dopant to produce ZnO based DMS. Understanding the mechanism of ferromagnetism in non-TM-doped ZnO is useful in exploring new areas of dilute magnetic semiconductors. In this Letter, we present our computational and experimental studies on ZnO films doped with carbon and show that carbon-doped ZnO can be a promising DMS.

First-principles calculations based on the density functional theory were carried out to investigate carbon doping of ZnO. Calculations were performed using the Vienna *ab initio* simulation package [13]. The projector augmented wave potentials [14] were used for electron-ion interactions and the local spin density approximation (LSDA) [15,16] was used to describe the exchange-correlation functional. The system was modeled with a periodic supercell of $9.553 \times 9.553 \times 10.222 \text{ \AA}^3$ with 18 f.u. of wurtzite ZnO, which is sufficient to avoid the interaction of the C atom with its images in neighboring supercells. An energy cutoff of 282.6 eV was used for the plane wave expansion of the electronic wave function. Special k points were generated with a $3 \times 3 \times 2$ grid based on the Monkhorst-Pack scheme [17]. Good convergence was obtained with these parameters, with the total energy converged to 1.0×10^{-4} eV/atom. The calculated lattice constants ($a = 3.184 \text{ \AA}$, $c = 5.111 \text{ \AA}$) for bulk ZnO are in good agreement with the experiment values ($a = 3.25 \text{ \AA}$, $c = 5.21 \text{ \AA}$) [18]. The calculated band gap is 0.835 eV within LSDA, which is consistent with the reported results [19,20]. We consider three types of carbon doping: carbon interstitial (C_i), carbon substitution at the Zn site (C_{Zn}) and carbon substitution at the oxygen site (C_O). The structure of carbon-doped ZnO was fully relaxed in our LSDA calculation using the conjugate gradient method until the Hellman-Feynman force was smaller than 0.01 eV/\AA .

Our calculations predicted magnetism in carbon-doped ZnO and revealed that it results from carbon substitution for oxygen. Figure 1 shows the calculated local density of states (LDOS) for the carbon dopant and the neighboring Zn atoms. Strong coupling between the carbon s and p orbitals and the s orbital of Zn can be seen. The interaction causes the carbon $2s$ orbital around -9 eV and the carbon $2p$ orbital near 2.3 eV to split. The spin-up bands are fully occupied while the spin-down bands are partially filled, resulting in a magnetic moment of $2.02\mu_B$ per carbon

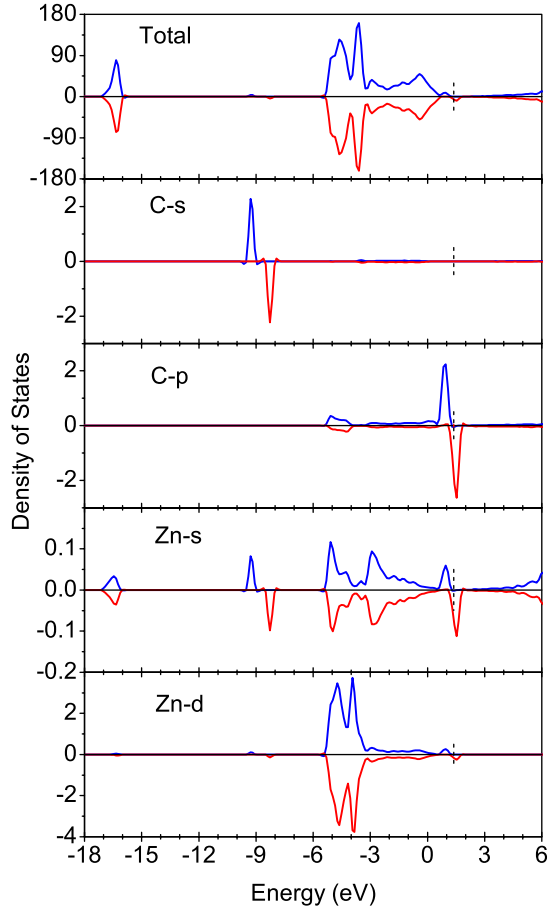


FIG. 1 (color online). Calculated total (top panel) and local density of states for the carbon dopant and a neighboring Zn atom. The Fermi level is indicated by the dashed vertical line.

dopant. The magnetic moment is mainly contributed by the carbon p orbitals ($0.85\mu_B$), while each of the neighboring Zn atoms and second nearest neighboring oxygen atoms also contribute a small part ($0.11\mu_B$ and $0.05\mu_B$, respectively), suggesting the Zn-C system as the origin of magnetism in C-doped ZnO. The estimated formation energy of the C_O defect is 5.3 eV, with respect to bulk ZnO and an isolated carbon atom. Similar calculations on carbon substitution for Zn and interstitial carbon showed that they do not result in magnetism.

To verify the theoretical prediction, we prepared C-doped ZnO films using pulsed-laser deposition (PLD). ZnO/ C_x targets with carbon concentrations $x = 0, 0.5, 1, 5,$ and 10 were prepared by sintering mixed ZnO (99.9%) and carbon (99.9%) powders in nitrogen atmosphere at 1273 K for 30 min. The base pressure was $<1 \times 10^{-8}$ torr. The C-doped ZnO films were deposited on sapphire (0001) substrate using a KrF excimer laser operating at 248 nm and a fluence of 1.8 J cm^{-2} . No ferromagnetism was found in the pristine ZnO, carbon powders, and sintered ZnO/C targets, as well as the substrates. The films were deposited at 673 K and a vacuum better than 10^{-7} torr in order to ensure epitaxial growth and avoid carbon loss during deposition. The carbon concentration was estimated based on the secondary ion mass spectrometry (SIMS) analysis with the support from x-ray photoelectron spectroscopy (XPS) and scanning electron microscopy examinations. The film thickness was chosen to be 200 nm in order to ensure an accurate estimation of magnetization and to minimize the substrate effect. Three samples with target carbon concentrations of 0, 1, and 5 at. %, designated as sample A, sample B, and sample C, respectively, were selected for the detailed structural and magnetic studies as listed in Table I.

Our x-ray diffraction study indicated that both pure and C-doped ZnO films had good epitaxy with the sapphire substrate. SIMS analysis showed that Zn and O are uniformly distributed in the C-doped films. The average carbon concentration was estimated to be 1 and 2.5 at. % for the ZnO + 1 and ZnO + 5 at. % C targets, respectively (Table I). It is noted that the carbon concentration in the film is lower than that in the target, and the carbon loss is severe when the carbon concentration in the target is higher ($>3-4$ at. %).

To investigate the states of doped C atoms, we carried out further analysis using XPS and Raman spectroscopy. Two groups of peaks in the C1s binding energy, namely, a large peak at 284.6 eV and a few peaks in the energy range of 280–284 eV were observed in the XPS analysis. The peak at 284.6 eV can be attributed to “free carbon” (graphite and/or carbon from contamination). Our Raman spectroscopic study confirmed the presence of graphite. The second carbon species with C1s binding energy be-

TABLE I. The properties of ZnO with and without carbon doping.

	Sample A	Sample B	Sample C
Carbon concentration of the target (at. %)	0	1	5
Measured C concentration (at. %)	...	~1	~2.5
Magnetization at 300 K (emu/cm^3)	0	5.1	7.1
Magnetization at 5 K (emu/cm^3)	0	7.2	10.1
Moment per C in carbide state	...	2.0–3.0	1.5–2.5
Resistivity ($\Omega \text{ cm}$)	4	0.195	0.108
Hall mobility ($\text{cm}^2/\text{V s}$)	94.2	22.6	14.5
Carrier concentration ($10^{18}/\text{cm}^3$)	0.1	2.1	3.8

tween 280 and 284 eV observed in the C-doped ZnO films suggests the presence of carbon atoms in the carbide form [21], indicating carbon substitution for oxygen and formation of Zn-C bonds in the carbon-doped ZnO films.

Magnetic properties of all three samples were investigated. As expected, the pure ZnO film without C doping is nonmagnetic, whereas both C-doped ZnO films show ferromagnetism at room temperature (inset in Fig. 2). A detailed magnetic and electronic investigation was carried out for the two samples—sample B with a relative low C-doping concentration and sample C with a high C-doping concentration. The temperature dependence of magnetization is shown in Fig. 2. The magnetization at 400 K is 3.8 emu/cm^3 for sample B, indicating that the Curie temperature of the film is higher than 400 K.

We also investigated the dependence of the measured saturation magnetization on carbon concentration in the samples, as shown in Fig. 3. The magnetization increases rapidly for low carbon concentrations (0–1 at. %), and becomes saturated when the carbon concentration in the target reaches about 5 at. % (2.5% in the sample). Assuming that the XPS peak at 284.6 eV is completely attributed to graphite carbon, we estimated the magnetic moment per carbon in the carbide form in the ZnO films and obtained values of $(2.5\text{--}3.0)\mu_B$ for sample B and $(1.5\text{--}2.5)\mu_B$ for sample C, respectively (Table I). Magnetic moments per carbon of other samples are plotted in Fig. 3. It can be concluded that the magnetic moment in the carbide form is in the range of $(1.5\text{--}3.0)\mu_B$ per carbon for all the C-doped samples, in agreement with the theoretical prediction of $2.02\mu_B$.

As reported previously [1], magnetoresistance (MR) and abnormal Hall effect (AHE) have been often observed in many DMSs. The AHE is an evidence of intrinsic ferro-

magnetism due to interactions between carriers and spins. In this Letter, we have studied AHE and MR of carbon-doped ZnO. Figure 4 shows the Hall effect of sample B at different temperatures. The total Hall effect can be expressed as $\rho_{xy} = R_0B + R_s\mu_0M$, where B is magnetic induction and M is the magnetization. The first term (R_0B) represents the ordinary Hall effect, whereas the second term ($R_s\mu_0M$) denotes the abnormal Hall effect. The normal Hall effect indicates that the film is an n -type semiconductor. The hysteresis loop of the Hall effect after the deduction of the normal Hall effect is shown in the inset. The shape of the Hall effect hysteresis loop is similar to that of the magnetic hysteresis loop as shown in Fig. 2. The Hall voltage strongly increases with the decrease of temperature. In addition, MR up to 0.5% was present in C-doped ZnO. MR was proportional to the measured magnetization.

To investigate the interaction between the magnetic moments, we carried out further calculations with two oxygen atoms substituted by carbons in the supercell, which corresponds to a doping concentration of 5.6%. The two substitutional C atoms were placed at the largest possible separation of 7.76 Å in the supercell, with the two magnetizations in ferromagnetic (FM) and antiferromagnetic (AFM) states, respectively. The atomic positions in each case were fully optimized and the total energy was calculated. It was found that the system remains half-metallic. The FM state is the ground state and its energy is 63 meV lower than that of the AFM state. This energy difference is larger than, for example, that of Cu-doped ZnO (42 meV) which is known to be ferromagnetic at room temperature [3,4]. Even though further studies may be required

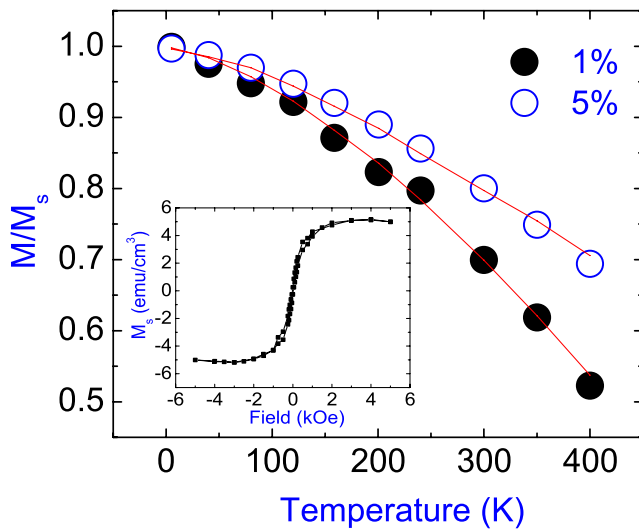


FIG. 2 (color online). $M_s(T)/M_s(5 \text{ K})$ versus temperature for samples B and C. The solid lines are a guide for the eye. The inset shows the hysteresis loop of sample B taken at 300 K.

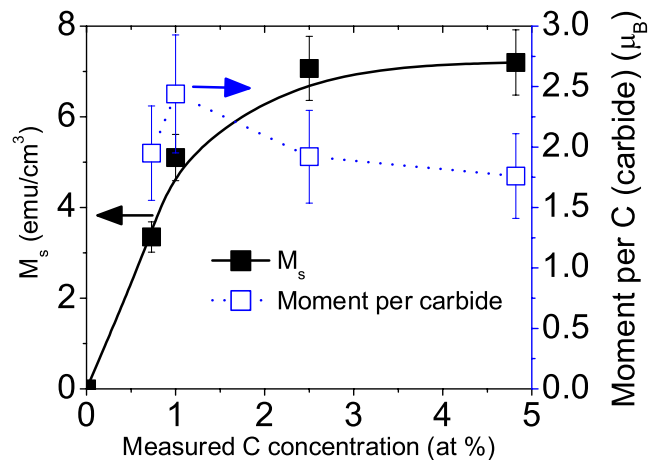


FIG. 3 (color online). The room-temperature saturation magnetization M_s and the magnetic moment per carbon in the carbide state (carbide carbon) as a function of the measured carbon concentration of the C-doped specimens. The carbon concentration in the sample was estimated by SIMS measurements, while the percentage of carbon in the carbide state was estimated by XPS measurements.

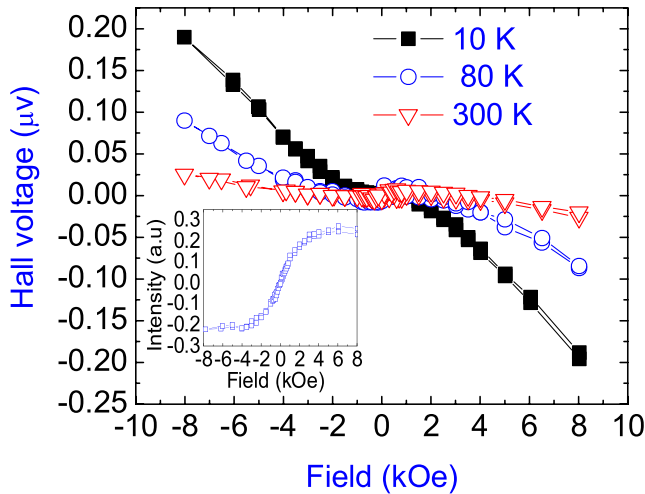


FIG. 4 (color online). The Hall voltage as a function of magnetic field for sample B at different temperatures. The inset shows the Hall effect curve at 10 K after the normal part is removed.

to fully understand the magnetic origin and coupling in this system, a mechanism similar to other DMSs such as (Ga,Mn)As and (Zn,Cu)O can be expected for ferromagnetism in carbon-doped ZnO. Based on the calculated band structures, we propose hole mediation as the mechanism of ferromagnetic coupling in C-doped ZnO. Substitution of C atoms at O sites in ZnO introduces holes in $O2p$ states, which couple with the parent $C2p$ localized spins by a $p-p$ interaction, similar to $p-d$ hybridization in TM-doped semiconductors or oxides. This $p-p$ interaction leads to the appearance of additional mixed band levels derived from the semiconductor valence band. The coupling “pushes” the minority $p-p$ mixed state upward and the opposite spin state downward, lowering the total energy of the system. The wave function of the $C2p$ states is spatially extended to neighboring $O2p$ states, and couple to the $O2p$ states. By this $p-p$ interaction, holes mediate the spin alignment of parent C atoms, leading to an indirect ferromagnetic coupling of C atoms. Compared to $p-d$ hybridization, the $p-p$ interaction is relatively long ranged, which may explain why a C-doping concentration as low as 1% induces significant ferromagnetism in ZnO. Even though our experimental results indicate that the majority carrier in the C-doped ZnO is electron, due possibly to the existence of free carbon and other types of defects such as oxygen vacancy, there should exist a sufficient number of minority carriers, i.e., holes, at finite temperature to mediate the spin alignment. It is also noted that the defect levels

in the minority spin are very close to the bottom of conduction band and electrons in the defect levels can be easily ionized, leaving holes behind. Our further calculations show that hole doping enhances ferromagnetism. For example, by codoping with C and N, both substituting O, the magnetic moment is increased by $\sim 1\mu_B$ per C dopant, further confirming hole-mediated ferromagnetism.

In conclusion, we demonstrated, both theoretically and experimentally, that C-doped ZnO is ferromagnetic at room temperature. Carbon-doped ZnO films show an intrinsic n -typed ferromagnetic behavior, with Curie temperatures well above room temperature. The intrinsic ferromagnetism originates from the Zn-C system in the ZnO environment. Our work demonstrates that carbon is a novel dopant in the class of doped ZnO dilute magnetic semiconductor materials.

Y.P. Feng wishes to thank Zhenyu Zhang for useful discussion on the topic, and acknowledges financial support from the National University of Singapore Academic Research Fund under Grant No. R-144-000-182-112.

*scip1124@nus.edu.sg

†phyfyp@nus.edu.sg

*msedingj@nus.edu.sg

- [1] T. Dietl *et al.*, *Science* **287**, 1019 (2000).
- [2] R. Q. Wu *et al.*, *Appl. Phys. Lett.* **89**, 062505 (2006).
- [3] L. H. Ye, A. J. Freeman, and B. Delley, *Phys. Rev. B* **73**, 033203 (2006).
- [4] D. B. Buchholz *et al.*, *Appl. Phys. Lett.* **87**, 082504 (2005).
- [5] J.-H. Lee *et al.*, *Appl. Phys. Lett.* **90**, 032504 (2007).
- [6] Y. Kopelevich *et al.*, *Phys. Rev. B* **68**, 092408 (2003).
- [7] A. V. Rode *et al.*, *Phys. Rev. B* **70**, 054407 (2004).
- [8] P. Esquinazi *et al.*, *Phys. Rev. Lett.* **91**, 227201 (2003).
- [9] S. Talapatra *et al.*, *Phys. Rev. Lett.* **95**, 097201 (2005).
- [10] H. Ohldag *et al.*, *Phys. Rev. Lett.* **98**, 187204 (2007).
- [11] P. O. Lehtinen *et al.*, *Phys. Rev. B* **69**, 155422 (2004).
- [12] R. Q. Wu *et al.*, *Appl. Phys. Lett.* **86**, 122510 (2005).
- [13] G. Kresse and J. Furthmüller, *Comput. Mater. Sci.* **6**, 15 (1996); *Phys. Rev. B* **54**, 11 169 (1996).
- [14] P. E. Blöchl, *Phys. Rev. B* **50**, 17953 (1994).
- [15] U. von Barth and L. Hedin, *J. Phys. C* **5**, 1629 (1972).
- [16] M. M. Pant and A. K. Rajagopal, *Solid State Commun.* **10**, 1157 (1972).
- [17] J. Monkhorst and J. Pack, *Phys. Rev. B* **13**, 5188 (1976).
- [18] O. Madelung, *Numerical Data and Functional Relationships in Science and Technology* (Springer-Verlag, Berlin, 1982), Vol. 17.
- [19] A. F. Kohan *et al.*, *Phys. Rev. B* **61**, 15 019 (2000).
- [20] Y. N. Xu and W. Y. Ching, *Phys. Rev. B* **48**, 4335 (1993).
- [21] L. Ramqvist *et al.*, *J. Phys. Chem. Solids* **30**, 1835 (1969).